

Effects of Resonant and Continuum States on the Neutrino-Nucleus Cross Section.

O. Civitarese^{1*}, R. J. Liotta² and M. E. Mosquera³

¹*Dept of Physics, University of La Plata c.c. 67 1900, La Plata, Argentina*

²*KTH, Albanova University Center, SE-10691 Stockholm, Sweden and*

³*Faculty of Astronomy and Geophysics, University of La Plata, La Plata, Argentina*

(Dated: December 13, 2018)

Estimates of the neutrino-nucleus cross section, for the charged-current process $\nu + {}^{208}\text{Pb} \rightarrow e^- + {}^{208}\text{Bi}^*$, are presented. The nuclear structure calculations have been performed by considering bound, resonant, and continuum states in the single-particle basis used to construct correlated proton-particle neutron-hole configurations. The observed features of the spectrum of ${}^{208}\text{Bi}$ have been reproduced, as accurately as possible, by diagonalizing a phenomenological multipole-multipole interaction. Calculations of the cross section, for values of $q \leq 200$ MeV, were performed, and the dependence of the results upon the choice of the residual proton-neutron interaction was investigated. It is found that the inclusion of resonant states in the calculation of the nuclear wave functions increases the neutrino-nucleus cross section, and that the contribution of the continuum is negligible.

PACS numbers: 26.30.Jk, 26.50.+x, 21.60.-n

key words: neutrino-nucleus cross section, nuclear structure, resonant states.

I. INTRODUCTION

During the last decade an intense effort, both theoretical and experimental, was devoted to elucidate neutrino properties and the connection between them and the physics of supernova [1, 2, 3]. The phenomena of neutrino oscillations was confirmed [4, 5], and with it, the solution of the solar neutrino problem [6, 7] was found. This is a cornerstone upon which we base our present knowledge of neutrino properties, and it will certainly be followed by other breakthroughs in other neutrino-related fields, like nuclear double-beta-decay [8] and neutrino astrophysics [9]. The prospect of detecting supernova-neutrino-flavor oscillations by analyzing the response of various nuclei to neutral- and charged-current interactions, was advanced by Fuller, Haxton and McLaughlin [10], and later pursued by Elliot [11] and Engel, McLaughlin and Volpe [13]. In these processes an electron-neutrino interacts inelastically with a target nucleus, leaving it in an excited state (neutral-current interactions), or it is absorbed and changes a neutron into a proton, thus resulting in an outgoing electron and a residual nucleus with charge $Z_f = Z + 1$ (charged-currents). For the case of charged-current interactions, that is the (ν_e, e^-) channels, the theoretical estimate of the total inelastic cross section varies from 10^{-40} cm², in the case of the process ${}^{23}\text{Na}(\nu_e, e^-){}^{23}\text{Mg}$, to 10^{-38} cm² for the case of ${}^{208}\text{Pb}(\nu_e, e^-){}^{208}\text{Bi}$ [10].

The lepton sector of the reaction is described in terms of a single-flavor neutrino (ν_e) to which we may add mixing terms due to neutrino oscillations [13]. The nuclear structure sector is governed by the strength distribution of the complete set of multipole excitations induced by the energy-momentum transferred from the lepton sector to the hadronic sector. A realistic description of the neutrino-nucleus cross section requires a fairly detailed knowledge of the nuclear spectrum [11, 14, 15], a goal which may be achieved by a direct diagonalization of the realistic nuclear interaction or by approximate methods like the Tamm-Dancoff Approximation (TDA) or the Random Phase Approximation (RPA). An alternative to the use of individual nuclear states is the use of energy-weighted sum rules and, subsequently, the replacement of the detailed nuclear-energy-level distribution by a few energy-centroids which concentrate all of the intensity carried by each multipolarity [15]. Though the low energy sector of the nuclear spectrum may be determined experimentally, thus allowing for a detailed comparison with theoretical predictions, the high energy part of it may be unreachable by standard spectroscopic methods and therefore it is not so well established theoretically, from the nuclear structure point of view. However, future measurements on neutrino-nucleus interactions may improve our knowledge on this high energy regime, as suggested by Volpe [16].

Lead perchlorate was suggested, as a detector of choice [11] because the estimated neutrino-nucleus cross section may be one or two orders of magnitude larger than the one corresponding to the scattering of neutrinos by ${}^{23}\text{Na}$. Also, future experimental efforts at SNOLAB, like HALO, will be based on neutrino reactions on Pb [12]. However, in

* Corresponding author
e-mail: osvaldo.civitarese@fisica.unlp.edu.ar

the case of lead, one encounters additional complications caused by the description of the spectrum of a double-odd-mass heavy-nucleus, like ^{208}Bi . In addition to the relatively well known strength distribution of the Isobaric Analog State (IAS) and Gamow-Teller (GT) resonances one should consider forbidden transitions leading to unnatural parity states. From the microscopic point of view one needs to calculate the eigenstates of the nuclear Hamiltonian belonging to complete sets of angular momentum J and parity π . It is evident that an exact shell model diagonalization can not be performed for a heavy-mass nucleus in a large model space. Thus, one may resort to approximations like weak-coupling schemes or TDA (RPA) treatments [17]. Because the energy deposited in the nucleus by the neutrino may be of the order of few tens to few hundreds of MeV, one may expect that the contribution of nuclear states in the continuum should also be considered, and, therefore, be added to the contributions resulting from the low energy region of the nuclear spectrum [14]. However, continuum RPA calculations find a serious discrepancy between measured and calculated cross sections for neutrino induced reactions [18, 19].

The role of neutrino induced reactions on lead and iron was discussed in a series of RPA calculations [20]. The formalism of [20] takes into account the correct momentum dependence of the operators entering the definition of the charge-current interactions, a fact leading to a reduction of the calculated values as compared with calculations performed at $q = 0$. The calculations of the various channels entering inclusive neutrino-nucleus interactions, of [20, 21], yield values of the cross section, for lead targets, which are dominated by neutron-emission processes from ^{208}Bi . This feature, which emerges from the results of [20] corresponding to LSND pion-decay in-flight neutrino energies and supernovae neutrinos, indicates that the contribution of the neutron emission channel is typically few orders of magnitude larger than the calculated γ and proton-emission channels. The contributions coming from proton emission from ^{208}Bi are significantly smaller, of the order of 10^{-41}cm^2 , than the neutron-emission channel, of 10^{-38}cm^2 . The contribution of the γ emission from ^{208}Bi amounts also to a fraction of the cross section, of 10^{-39}cm^2 . The smallness of the contribution of the proton-emission channel is particularly interesting, since one may expect that the proton emission from isovector resonances (mostly Isobaric Analogue and Gamow-Teller states) may be significant [22].

In dealing with the theoretical description of processes involving the continuum part of nuclear spectra one has to distinguish among the various approaches that have been used for this purpose. One can thus mention: 1) the analytical extension of the discrete portion of the spectrum [18]; ii) the continuum shell model [24] and iii) the shell model in the complex energy plane (CXSM) [25]. The CXSM has been used extensively since its first application nearly 20 years ago [26]. It will also be applied in this paper. A brief description of its main ingredients will be given in the next Section.

In the context of the neutrino-nucleus scattering, the nuclear structure component of the calculation will then be centered upon the theoretical prediction of the distribution of intensities for the nuclear transitions induced by the multipole operators of the leptonic current. Because the energy transferred to the nucleus may be large, of the order of 100-200 MeV, the probability to excite nuclear states with a large component on a single-particle resonance is also very large. This fact then opens the possibility of finding enhancement of the cross section, similarly to the one found in proton-emission and in cluster-emission.

In this work we have calculated neutrino-nucleus cross sections on lead, leading to ^{208}Bi , including resonant and continuum states in the single-particle basis. In so doing we focus our attention on the possible effects due to the inclusion of the continuum. For the sake of the present calculation, we aim at a quantitative estimate of the contributions due to the continuum, by performing nuclear structure calculations in Berggren's representation [26, 28, 29]. As we shall show, the effects associated to the inclusion of the nuclear continuum are extremely small. Contrary to this, the inclusion of single-particle resonances increases the cross section significantly.

The formalism of the neutrino-nucleus interactions is briefly reviewed in Section II A. Details about the nuclear structure calculations are presented in Section II B. The results of the calculations are discussed in Section III. Finally, the conclusions are drawn in Section IV. Details of the theoretical formulations are presented in the Appendixes A, B, and C.

II. FORMALISM

In this section we will present the essentials of the formalism, which includes two main components: a) the treatment of neutrino-nucleus interaction, and, b) the use of nuclear models to calculate the participant nuclear wave functions. We shall focus on the process

$$\nu + ^{208}\text{Pb} \rightarrow e^- + ^{208}\text{Bi}^*, \quad (1)$$

thus we have to calculate explicitly an electroweak process, where the incoming neutrino ν decays into an electron- W boson-pair, followed by the nuclear conversion of a neutron into a proton and the absorption of the W^+ boson in the target nucleus, leading to excited state of the final nucleus ^{208}Bi .

A. Charged-Current Neutrino-Nucleus Interactions

The cross section for the inelastic neutrino-nucleus interaction in the charged current channel is written

$$\sigma = (2\pi)^4 \sum_f \int d^3 p_l \delta(E_l + E_f - E_\nu - E_i) |\langle l(p_l); f | H_{eff} | \nu(p_\nu); i \rangle|^2, \quad (2)$$

where $|\nu(p_\nu); i \rangle$ is the initial product state of the incoming neutrino ν , with momentum p_ν , and the ground state of the target nucleus ^{208}Pb , E_i is the energy of the ground state of ^{208}Pb , $|l(p_l); f \rangle$ is the product state of the outgoing lepton l (e^-) of momentum p_l and the excited state f belonging to the complete set of states of ^{208}Bi , with angular momentum J_f , parity π_f and energy E_f . In the convention which we have adopted the energy E_f is measured respect to the ground state of ^{208}Pb , E_l is the energy of the outgoing lepton (electron), E_ν is the energy of the incoming neutrino, and H_{eff} is the electroweak interaction. After separation of the leptonic and hadronic components of the current-current interaction, H_{eff} , one gets [14]

$$\sigma = \frac{G^2}{\pi} \cos^2 \theta_C \sum_f p_l E_l F(Z_f, E_l) \frac{1}{2} \int_{-1}^1 d(\cos \theta) M_{\text{Nuc}}. \quad (3)$$

The elements of this equation are the electroweak coupling constant G , the Cabibbo angle θ_C , the energy and momentum of the outgoing lepton (E_l, p_l), the Fermi function $F(Z_f, E_l)$ [27], and the nuclear transition probability M_{Nuc} . The sum runs over the complete set of nuclear states $|f \rangle$ of ^{208}Bi , and the variable of integration is the angle between the incoming neutrino and the outgoing lepton. By expanding the hadronic weak current in powers of the inverse nucleon-mass M_N^{-1} , and keeping the non-relativistic limit of small momenta, that is $p_N/M_N \ll 1$, where p_N is the momentum of the nucleon, one obtains the standard operators which induce momentum-dependent axial-vector, vector, weak-magnetic and pseudoscalar transitions [17]. The nuclear transition probability M_{Nuc} may, therefore, be decomposed into allowed Fermi and Gamow-Teller transitions, and forbidden and allowed transitions of higher multiplicities.

The explicit expressions of the components of the nuclear transition probability M_{Nuc} are

$$M(\tau) = |\langle f | \tau_- e^{iqr} | i \rangle|^2 = \frac{4\pi}{2J_i + 1} \sum_l \left| \langle J_f^\pi || \sum_k \tau_-(k) i^l j_l(qr_k) Y_l(\hat{\mathbf{r}}_k) || J_i^\pi \rangle \right|^2, \quad (4)$$

for the isospin dependent operators, and

$$M(\sigma\tau) = |\langle f | \sigma\tau_- e^{iqr} | i \rangle|^2 = \frac{4\pi}{2J_i + 1} \sum_{l,K} \left| \langle J_f^\pi || \sum_k \tau_-(k) i^l j_l(qr_k) [Y_l(\hat{\mathbf{r}}_k) \times \sigma(k)]^{(K)} || J_i^\pi \rangle \right|^2, \quad (5)$$

for the spin-isospin dependent operators. To these terms one adds the moment

$$\begin{aligned} M(\Lambda) &= \left(\frac{5}{6}\right)^2 \frac{4\pi}{(2J_1 + 1)} \sum_{l,l',K} (-1)^{l/2-l'/2+K} \sqrt{(2l+1)(2l'+1)} \begin{pmatrix} l & l' & 2 \\ 0 & 0 & 0 \end{pmatrix} \begin{Bmatrix} 1 & 1 & 2 \\ l' & l & K \end{Bmatrix} \\ &\times \langle J_f^\pi || \sum_k \tau_-(k) i^l j_l(qr_k) [Y_l(\hat{\mathbf{r}}_k) \times \sigma(k)]^{(K)} || J_i^\pi \rangle \\ &\times \langle J_f^\pi || \sum_{k'} \tau_-(k') i^{l'} j_{l'}(qr_{k'}) [Y_{l'}(\hat{\mathbf{r}}_{k'}) \times \sigma(k')]^{(K)} || J_i^\pi \rangle^* \end{aligned} \quad (6)$$

The total nuclear matrix element of Eq.(3) includes weak-magnetic and pseudoscalar contributions (see [15] for details), and it is written

$$M_{\text{Nuc}} = \lambda_\tau M(\tau) + \lambda_{\sigma\tau} M(\sigma\tau) + \lambda_\Lambda M(\Lambda) \quad (7)$$

The quantities λ_τ , $\lambda_{\sigma\tau}$, and λ_Λ are functions of the momentum and direction of the outgoing electron and of the nucleon form factors. Their explicit expressions are given in Refs. [14] and [15] and in Appendix C. In the above equations $q = p_l - p_\nu$ is the momentum transferred from the leptonic to the nuclear sectors, and τ_- transforms a neutron into a proton. The transitions induced by the multipole operators of Eqs.(4) and (5) obey the standard selection rules of the conservation of total angular momentum for parity-changing operators (generally speaking forbidden transitions) and parity conserving operators (allowed transitions).

B. Nuclear Structure Calculations with Resonant and Continuum States

We write the wave function of the excited k -th member of the J^π multiplet in ^{208}Bi as the superposition of particle(proton)-hole(neutron) states

$$|JM, k\rangle = \sum_{pn} C^{(k)}(pn, J^\pi) |pn^{-1}; JM\rangle. \quad (8)$$

and determine the amplitudes $C^{(k)}(pn, J^\pi)$ by a direct diagonalization of the residual two-body interaction in the proton-particle-neutron-hole space. The neutron-hole states are bound-states but the proton-particle states may be bound-, resonant- or continuum-states.

The single-particle basis which includes all of these possibilities is an extension of the conventional single-particle basis and its use in nuclear structure calculations was advocated long ago [26]. The calculation of nuclear wave functions and transition densities (Appendix B) in this basis constitutes a mayor difference with respect to previous calculations [10, 11, 13, 14, 15], where only bound states have been included in the single-particle basis. The expressions of the matrix elements of the two-body residual interaction, which we have chosen as to reproduce the spectrum of ^{208}Bi , are given in the Appendix B. Hereafter we shall review briefly the concepts and general aspects of the definition of the single-particle with bound, resonant and continuum states. This single-particle basis, which forms the Berggren representation, has been described before e. g. in Refs. [26, 28, 29]. We will give here only a brief summary of the formalism.

The regular solutions of the Schrödinger equation with outgoing boundary conditions corresponding to a particle moving in a central potential provide the single-particle bound states and complex states. The complex states may or may not have physical meaning but they (as well as the bound state) are poles of the single-particle Green-function. Since at large distances they behave as e^{ikr} in the complex k -plane one can uniquely classify them in four categories, namely:

- 1) bound states, for which $\text{Re}(k)=0, \text{Im}(k)>0$,
- 2) anti-bound states, for which $\text{Re}(k)=0, \text{Im}(k)<0$.
- 3) outgoing (decay) states for which $\text{Re}(k)>0, \text{Im}(k)<0$,
- 4) incoming (capture) states for which $\text{Re}(k)<0, \text{Im}(k)<0$.

One sees that only bound states do not diverge at large distances. One may therefore conclude that only the bound states are physically meaningful. However, if the wave functions corresponding to the complex poles are localized, they either correspond to resonances or anti-bound states which can be observed or which can produce observable effects [30]. We will analyze this feature with some detail in the Applications below.

In a pioneering paper [28] Berggren obtained an expansion of the Green- and δ -functions in terms of the poles of the Green-function plus an integral along a continuum path in the complex energy plane, i. e.

$$\delta(r-r') = \sum_n w_n(r)w_n(r') + \int_{L^+} dE u(r, E)u(r', E) \quad (9)$$

The summation runs over all bound states and poles of the Green function enclosed by the real E -axis and the contour L^+ . One can choose quite general forms for the contour, as can be seen in Ref. [31], but it has to finish at infinite on the real energy axis. However, as in any shell-model calculation, one cuts the energies at a certain maximum value. As a direct illustration of these concepts we shall refer the reader to Ref. [30] particularly for details concerning the integration contour L^+ .

In Eq. (9) the scattering functions on the contour are denoted by $u(r, E)$ while the wave functions of the bound single-particle states and the Gamow resonances are denoted by $w_n(r)$.

An important feature in Eq. (9) is that the scalar product is defined as the integral of the wave function times itself, and not its complex conjugate. This is in agreement with the Hilbert metric on the real energy axis since for bound states or for scattering states on this axis one can choose the phases such that the wave functions are real quantities. The prolongation of the integrand to the complex energy plane, which is done by applying the Cauchy theorem, allows one to use the same form for the scalar product everywhere. This metric (Berggren metric) produces complex probabilities, as has been discussed in detail in e. g. Ref. [32]. Here it is worthwhile to point out that for narrow resonances such probabilities become virtually real quantities.

The integral in Eq.(9) can be discretize such that

$$\int_{L^+} dE u(r, E)u(r', E) = \sum_p h_p u(r, E_p)u(r', E_p) \quad (10)$$

where E_p and h_p are defined by the procedure one uses to perform the integration. In the Gaussian method E_p are the Gaussian points and h_p the corresponding weights. Therefore the orthonormal (in the Berggren metric) basis vectors $|\varphi_j\rangle$ are given by the set of bound and Gamow states, i. e. $\langle r|\varphi_n\rangle = \{w_n(r, E_n)\}$ and the discretize scattering states, i. e. $\langle r|\varphi_p\rangle = \{\sqrt{h_p}u(r, E_p)\}$. This defines the Berggren representation.

III. RESULTS AND DISCUSSIONS

A. Nuclear Structure of Bi

The first step in the present calculations is the construction of the single-particle basis. For this we have diagonalized the Woods-Saxon plus Coulomb potential to which we have added a spin-orbit term. The parameter of the single-particle hamiltonian have been taken from [33]. The calculation of the single-particle states corresponding to all poles were performed by using the method and computer codes of Ref. [34]. In order to illustrate the typical values of the real and imaginary parts of the energies corresponding to the proton states thus evaluated we present in Table 1 some selected cases. The actual single particle basis extends over 136 proton states, with 5 bound states, 4 quasi-bound states, 10 narrow resonant states and 117 continuum states. We chose the contour containing the resonances such that they have physical meaning, i. e. that they are localized inside the nucleus. In other words, the proton is trapped by the Coulomb and centrifugal barriers inside the nucleus and therefore the corresponding wavefunction should also be concentrated inside the nucleus. This wavefunction looks like the wavefunction corresponding to a bound state (it is practically a real function) up to large values of the radius. This large distance depends upon the high of the barrier. The higher the barrier the larger the distance. Beyond it the wavefunction (including its imaginary part) starts to diverge. Thus, our contour does not include poles of the Green function which are very far from the real energy axis. Such poles cannot be considered resonances but rather they are a part of the continuum background. Their contribution (as well as the contribution of any physical resonance which might be left outside the contour) will be taken into account by the scattering states in the contour. An example of a non-resonant state is the $g_{9/2}$ pole at (17.838,-3.546) MeV shown in Fig. 1. One sees that this wave function is small inside the nucleus and that it starts

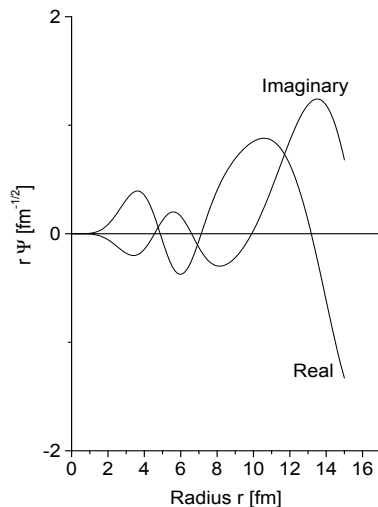


FIG. 1: Real and imaginary parts of the radial wave function (times r) corresponding to a proton state $g_{9/2}$ lying at (17.838,-3.546) MeV, i. e. deep in the continuum.

to diverge just outside the nuclear surface, which in this case is located at $r \approx 7.5$ fm. The imaginary part is as large as the real part. This is not a physical state but a part of the continuum background.

The neutron basis includes 16 single-particle bound states bellow the N= 126 shell-closure. With these states we have, as a next step, constructed unperturbed particle-hole states for configurations with total angular momentum J and parity π ($J^\pi \leq 10^\pm$), and diagonalized the interaction (given in B1) in the proton (particle)-neutron (hole) states. The couplings have been adjusted to reproduce the first excited state for each multipolarity. We have further verified

that the dominant configurations have coefficients similar to those of [35]. We have taken the comparison with the results of [35] as a consistency test of our single-particle basis. Table II shows the calculated values of the centroids

| lj | E (real) [MeV] | E (imag) [MeV] | |
|------------|----------------|----------------|-------------|
| $h_{9/2}$ | -3.784 | 0 | bound |
| $f_{7/2}$ | -3.541 | 0 | bound |
| $i_{13/2}$ | -1.844 | 0 | bound |
| $p_{3/2}$ | -0.690 | 0 | bound |
| $f_{5/2}$ | -0.518 | 0 | bound |
| $p_{1/2}$ | 0.491 | 0 | quasi-bound |
| $g_{9/2}$ | 4.028 | 0 | quasi-bound |
| $i_{11/2}$ | 5.434 | 0 | quasi-bound |
| $j_{15/2}$ | 5.960 | 0 | quasi-bound |
| $d_{5/2}$ | 6.748 | -0.002 | resonant |
| $s_{1/2}$ | 7.843 | -0.037 | resonant |
| $g_{7/2}$ | 8.087 | -0.001 | resonant |
| $d_{3/2}$ | 8.530 | -0.028 | resonant |
| $f_{7/2}$ | 12.748 | -0.652 | resonant |
| $h_{11/2}$ | 11.390 | -0.022 | resonant |
| $k_{17/2}$ | 14.066 | -0.001 | resonant |
| $h_{9/2}$ | 15.964 | -0.393 | resonant |
| $j_{13/2}$ | 15.086 | -0.005 | resonant |
| $i_{13/2}$ | 18.143 | -0.575 | resonant |

TABLE I: Proton bound, quasi-bound and resonant states, above the closure $Z=82$. The values given in columns are the real and imaginary parts of the energy, in units of MeV.

corresponding to the set of 0^+ and 1^+ states included in the calculations. Each set of states exhausts the Ikeda's sum rule at the 1 – 4% level (real part), given a further indication about the rightness of the approach concerning the combined effects of bound, resonant and continuum states.

| J^π | Energy (Real) [MeV] | Energy (Imaginary) [MeV] |
|---------|---------------------|--------------------------|
| 0^+ | 15.21 | -0.125 |
| 1^+ | 16.07 | -0.171 |

TABLE II: Energy-centroid for $J^\pi = 0^+, 1^+$ excitations in ^{208}Bi . The calculated real and imaginary part of the energy-centroid, for each multipolarity, are given in the table.

The calculated energy-difference between the centroids for pure Gamow-Teller and Fermi transitions is of the order of 0.86 MeV, a value which compares rather well with the experimental splitting between the corresponding GT and IAS resonances, which for $A=208$ is of the order of 0.5 MeV. The calculated position of the GT resonance is $E_{\text{GTR}}=15.6$ MeV, thus the calculated energy difference between the GTR and the IAS is of the order 0.4 MeV, again agreeing with the corresponding experimental value within experimental limits. Concerning the total intensity, we have verified that the real part of the Ikeda sum rule is, for each case, much larger than the imaginary part. The ratio between the imaginary and real parts of the calculated Ikeda sum rule is of 1.5 % (for the GT transitions) and 3.5 % (for the Fermi transitions). This imaginary part can be interpreted as the uncertainty related to the interference between the resonances and the background [36].

B. The $(\nu.e^-)$ cross section

After having introduced the features of bound, quasi-bound, resonant and continuum states we shall present and discuss our results for the cross section (3). In performing our calculations, and analyzing the results, we have focussed on the following aspects:

- a) Dependence of the results upon the chosen residual proton-neutron interaction

In order to determine the order of magnitude of the cross section, an issue which may still be controversial in view of some recently published results [37], we have performed a detailed comparison between the nuclear structure calculations described before and those of [35]. The calculations of Ref. [35] are particularly accurate for the description of the low-energy portion (excitation energies lower than 3-4 MeV) of the spectrum of ^{208}Bi . By the other hand, the calculations performed by using the separable interaction introduced in the previous paragraphs are well suited for the description of the higher portion of the spectrum., since the parameters of the interaction have been adjusted in order to reproduce the position and intensity distribution of the Isobaric Analogue State (IAS) and Giant Gamow-Teller Resonance (GTR). However, since little is known about the energy distribution of other multipole states, some doubts may arise concerning the reliability of the calculated wave functions of other multiplicities. Figures (2) to (4) show the results which we have obtained by using both the δ -force interaction of [35], and the separable multipole-multipole interaction of Eq.(B1). This set of results correspond to the diagonalization of both interactions in a single particle basis which includes only bound and quasi-bound states. The similarity between the results is undeniable, adding confidence to the present results, which for the values of the momentum transferred considered agree also with the results of Volpe et al. [38].(see our Figs.(2) and (3) and Table 1 of [38], for $q=100$ MeV, that is $\sigma \approx 4.16 \times 10^{-38}$ cm² (of Ref. [38]) and $\sigma \approx 3.04 \times 10^{-38}$ cm² (present)).

b)Multipole decomposition

Figure 4 shows the contributions of all multipole states considered in our calculations, for some selected values of the momentum transferred. The comparison of the results shown in insets (a)-(d) of this figure indicates that both interactions yield to very similar results, and that the contributions reach a maximum at about $q = 100 - 150$ MeV. Both interactions show a sizeable contributions from the $J^\pi = 1^+$ states, among the positive parity states, and for the $J^\pi = 2^-, 3^-, 4^-$ states, for the negative parity states.

c)Effects due to the inclusion of resonant and continuum states

In Figure 5 we show the contributions of allowed Fermi and Gamow-Teller transitions to the cross section of Eq. (3). The calculations have been performed by keeping the different classes of states which define the single-particle basis. The curves labelled *bound*, *resonant*, and *continuum* indicate the contribution of configurations, of the nuclear wave functions, where the proton-particle state is a bound, resonant or continuum state. The results show a sizeable contribution of resonant states, which increases with the neutrino energy, and a negligible contribution from states in the continuum, in spite of the huge number of continuum states included. This is, somehow, an expected result, because the time scale involved in the decay of single-particle resonances is much larger than the time available for the energy transfer from the incoming neutrino. However, in Refs. [18, 19], it was speculated on that the continuum could play a significant role in neutrino-nucleus interactions, because of the increase of the cross section at energies of the order of 100 MeV. This is not what we have found consistently in all of our results. Also in the case of the forbidden transitions, the effect due to the inclusion of the continuum is minor.

Figure 6 shows the comparison of the results corresponding to bound, quasi-bound and resonant states. It becomes evident that the inclusion of resonant states increases significantly the values of the cross section, for momentum transfer higher than 100 MeV. One should notice that in getting these results we have not restricted the number of resonant states by keeping, for instance, very narrow resonances only. If one does it, the increase of the cross section at higher energies is smaller than the one shows in Figure 6, but still seizable. A noticeable feature of the curves of Figure 6 is the saturation of the cross section, at values of the order of $\sigma \approx 6 \times 10^{-38}$ cm² (bound and quasi-bound states) and $\sigma \approx 18 \times 10^{-38}$ cm² (bound, quasi-bound and resonant states).

As an overall feature, the contribution of the continuum-states is to be neglected since the bulk of the cross section is given by bound and resonant states.

IV. CONCLUSIONS

In this work we have calculated some of the processes which contribute to the cross section for neutrino charged-current interactions on lead. We focus on the γ and proton emission channels from ^{208}Bi . The nuclear structure part of the calculation was done by enlarging the single-particle basis to accommodate for bound, resonant and continuum single-particle states. In this enlarged basis we have calculated nuclear wave functions for states belonging to the spectrum of ^{208}Bi . The description of the nuclear states was performed by a direct diagonalization of an effective, separable, interaction with multipole strengths adjusted to the phenomenology. The quality of the adjusted interaction was established, also, by a direct comparison with the force employed by [35]. The cross section was calculated by performing a partial wave expansion of the lepton wave functions and by computing the matrix elements of isospin and isospin-spin multipole operators between the ground state of ^{208}Pb and excited states of ^{208}Bi .

The results of the calculations, show that : i) the largest contributions to the considered channels of the cross section are given by nuclear excitations where bound and resonant states participate as proton single-particle states, and ii) the contribution of single-particle states in the continuum is, for all practical purposes, negligible.

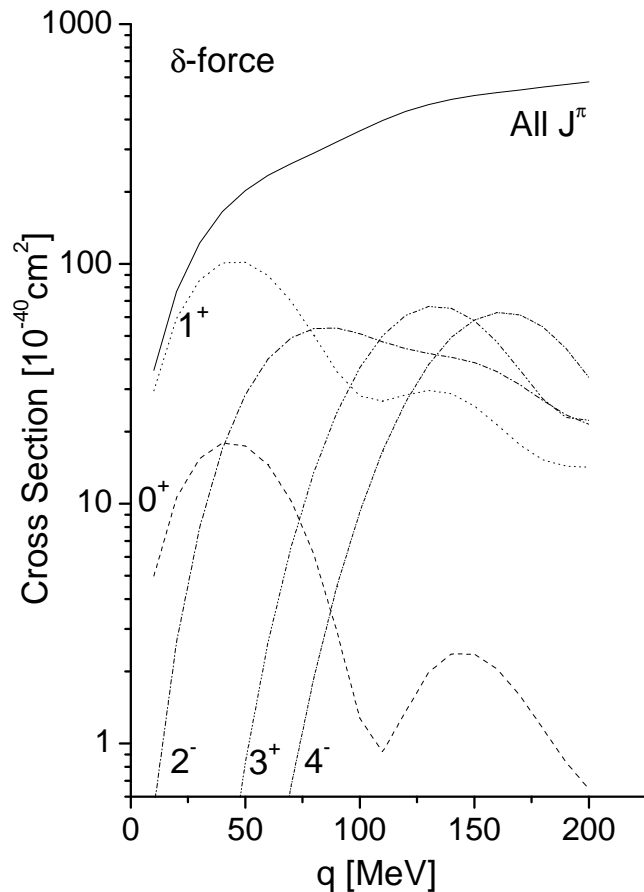


FIG. 2: Cross section, as a function of the momentum transferred by the neutrino. The results corresponding to nuclear structure calculations of states J^π in ^{208}Bi performed in an ordinary single particle basis and using a δ force interaction are shown. Solid line represents the results obtained by adding up all states up to $J^\pi \leq 10^\pm$, the other curves show the results of some selected states.

Although the results may be taken as a single-case sample, since we have considered just the case of neutrino-electron reaction on Pb, we think that they are representative of the situation which may emerge in neutrino reactions on other targets, like ^{12}C . Work is in progress concerning this light mass target.

Because of the structure of the nuclear transition operators involved in the calculations, we expect to find similar results in the description of single beta-decay processes. Work is in progress concerning single and double beta decay calculations with the inclusion of resonant single-particle states.

V. ACKNOWLEDGEMENT

This work has been partially supported by the National Research Council (CONICET) of Argentina. Discussions with Drs S. Elliott and K. Kubodera are acknowledged with pleasure. We are particularly indebted to Dr. Cristina Volpe, for her useful comments about the momentum dependence of the cross section, for helping in finding errors in an earlier version of the manuscript, and for her careful reading of the present version.

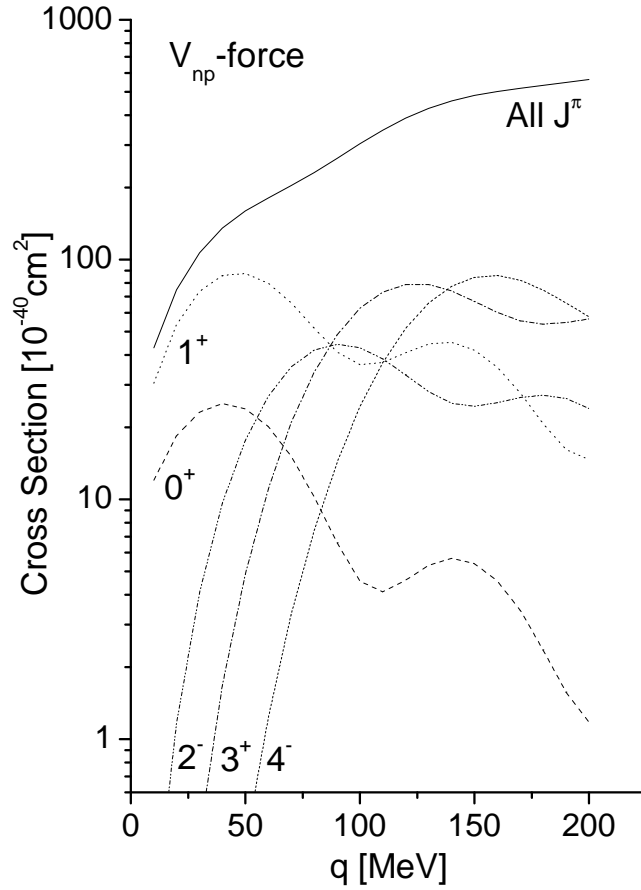


FIG. 3: Cross section, as a function of the momentum transferred by the neutrino. The results corresponding to nuclear structure calculations of states J^π in ^{208}Bi performed in the single particle basis which includes only bound and quasi bound states and using a separable multipole force interaction are shown. Solid line represents the results obtained by adding up all states up to $J^\pi \leq 10^\pm$, the other curves show the results of some selected states.

APPENDIX A: THE OPERATORS AND THEIR MATRIX ELEMENTS

The wave functions of single-particle states are written as the product of radial, orbital, and spin wave functions:

$$\Psi_{s,p} = R(r)i^l \left[Y_l(\hat{r})\chi^{1/2} \right]_{jm}. \quad (\text{A1})$$

where $R(r)$ is the radial part of the wave function, $Y_{lm_l}(\hat{r})$ is the orbital component of the angular momentum and $\chi_{m_s}^{1/2}$ is the spin component. The operators which enter the definition of the current-current electroweak interaction are written:

$$T_{(L,\gamma=1)\lambda\mu} = j_L(qr)i^L [Y_L \times \sigma]_{\lambda\mu} \tau_-, \quad (\text{A2})$$

for spin-dependent operators, and

$$T_{(L,\gamma=0)\lambda\mu} = j_L(qr)i^L Y_{\lambda=L,\mu=M_L} \tau_-, \quad (\text{A3})$$

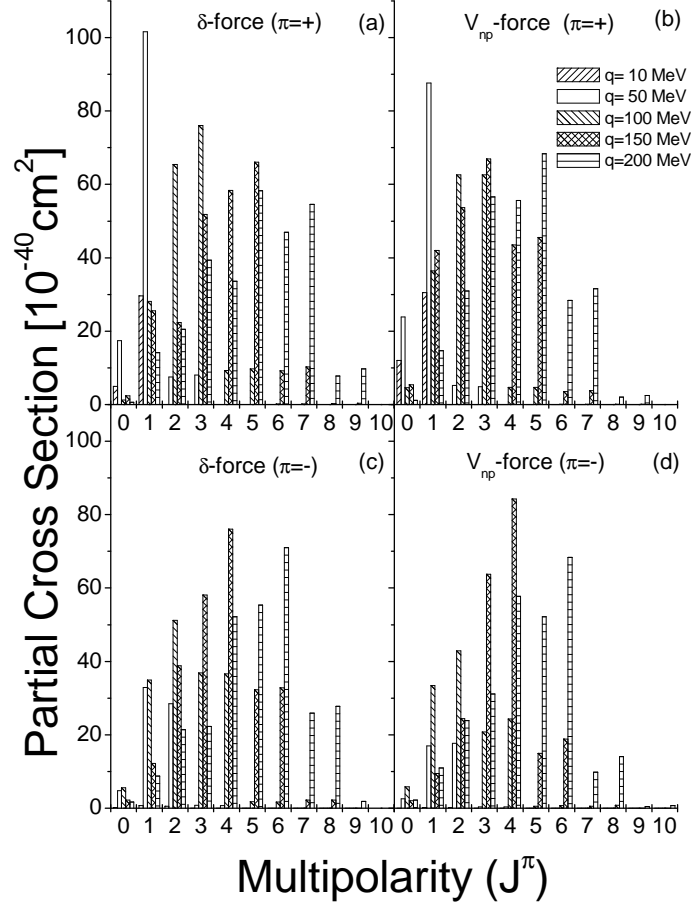


FIG. 4: Multipole decomposition of the contributions to the cross section, for some selected values of the momentum q . The upper insets (a) and (b) show the contributions of positive parity states, lower insets (c) and (d) show the results of negative parity states. The insets at the left, (a) and (c), show the results obtained by using a delta force interaction, right hand side insets (b) and (d) show the results obtained with a separable proton-neutron interaction, as explained in the text .

for spin-independent operators, $j_L(qr)$ is the regular Bessel function of integer order. The tensor operators can be expressed in terms of proton(particle)-neutron(hole) configurations as:

$$\begin{aligned}
 T_{\lambda\mu} &= \sum_{pn} \langle p | T_\lambda | \bar{n} \rangle a_p^\dagger a_{\bar{n}} \\
 &= \sum_{pn} \frac{\langle p || T_\lambda || n \rangle}{2\lambda + 1} (a_p^\dagger b_n^\dagger)_{\lambda\mu}.
 \end{aligned} \tag{A4}$$

In this notation the operator a^\dagger creates a proton and the operator b^\dagger creates a neutron-hole. The reduced matrix elements of the operators $F_{\lambda\mu}$ are given by the expression

$$\langle p || T_\lambda || n \rangle = F(pn, qL)G(pn, L\gamma\lambda), \tag{A5}$$

where

$$F(pn, qL) = \int dr r^2 R_p(r) j_L(qr) R_n(r), \tag{A6}$$

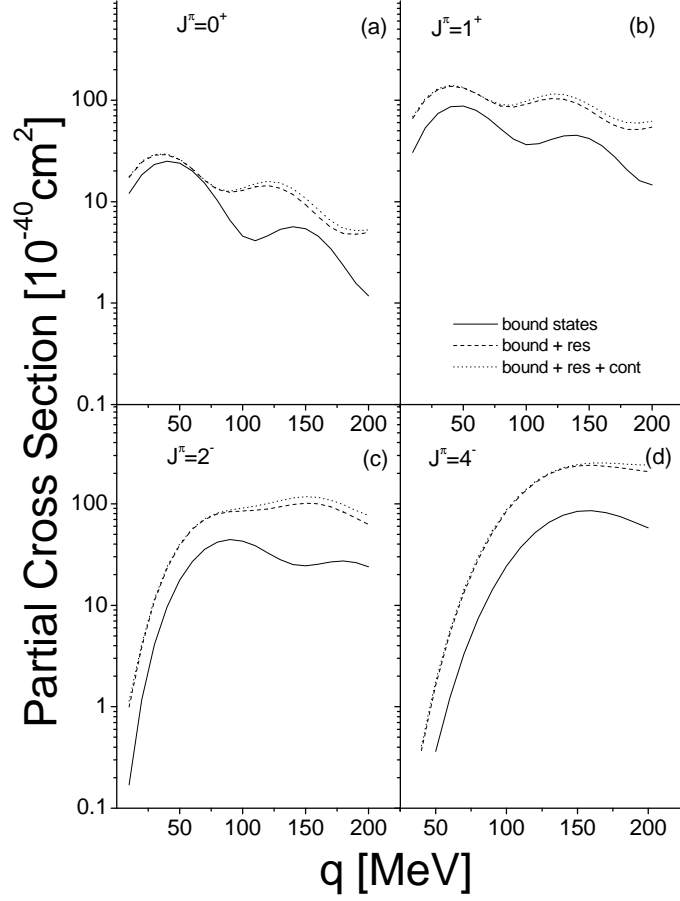


FIG. 5: Contributions to the cross section, for some selected multipole states, obtained with the separable multipole-multipole interaction. Insets (a)-(d) show the results corresponding to $J^\pi = 0^+, 1^+, 2^-,$ and 4^- states. Solid lines show the results of bound and quasi-bound states, dashed and dotted lines show the results obtained by including resonant states and scattering (continuum) states

and

$$G(pn, L\gamma = 1, \lambda) = \hat{\lambda} \hat{j}_n \hat{j}_p \hat{L} \hat{l}_n i^{l_n - l_p + L} \langle l_n 0 L 0 | l_p 0 \rangle \sqrt{\frac{3}{2\pi}} \left\{ \begin{matrix} l_n & 1/2 & j_n \\ L & 1 & \lambda \\ l_p & 1/2 & j_p \end{matrix} \right\}, \quad (\text{A7})$$

are the radial integral and the angular momentum re-coupling factors for spin-dependent operators ($\gamma = 1$), and

$$F(pn, qL) = \int dr r^2 R_p(r) j_L(qr) R_n(r), \quad (\text{A8})$$

and

$$G(pn, L\gamma = 0, \lambda = L) = \hat{j}_n \hat{j}_p \hat{L} \hat{l}_n i^{l_n - l_p + L} \langle l_n 0 L 0 | l_p 0 \rangle \sqrt{\frac{1}{8\pi}} (-1)^{j_n + 1/2 + l_p + L} \left\{ \begin{matrix} l_n & j_n & 1/2 \\ j_p & l_p & L \end{matrix} \right\}, \quad (\text{A9})$$

for spin-independent operators ($\gamma = 0$), respectively.

In the above equation $\hat{k} = \sqrt{2j_k + 1}$, and the adopted coupling scheme is always $|(ls)jm\rangle$ and the standard phases for the angular momentum re-couplings [39].

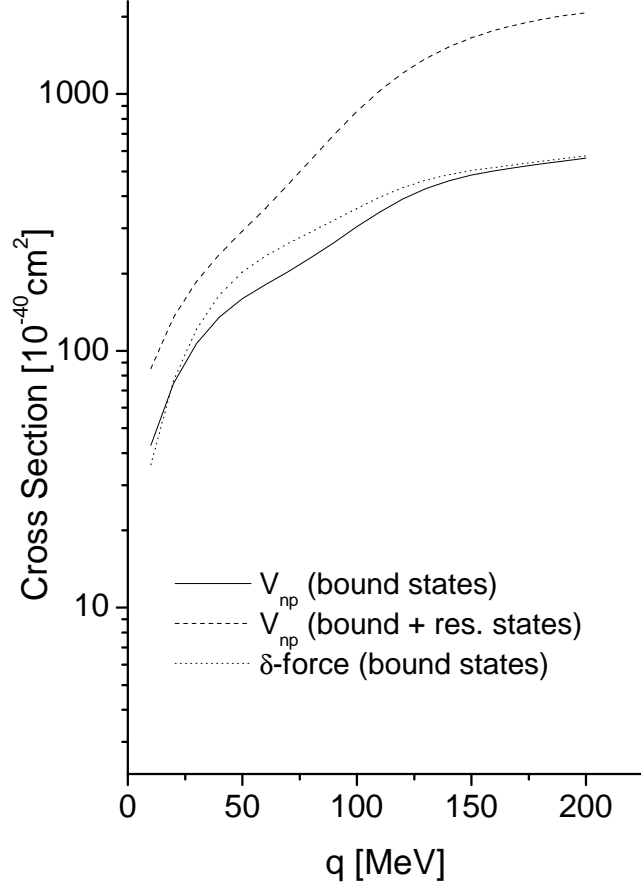


FIG. 6: Total cross section (sum over all multipoles and parities), as a function of the momentum q , corresponding to the separable interaction (solid line) and delta force interaction (dotted lines) in a basis of bound and quasibound states. The results corresponding to the separable interaction V_{np} , diagonalized in the basis which includes bound, quasibound and resonant states, are shown with dashed lines.

APPENDIX B: NUCLEAR TRANSITION DENSITY

The single particle basis has been constructed by including bound neutron states and bound, resonant and continuum proton states. We performed a TDA calculation of the spectrum of ^{208}Bi , by diagonalizing the interaction

$$V = \sum_{L\gamma\lambda} g_{L\gamma\lambda} (T_{L\gamma\lambda} \cdot T_{L\gamma\lambda})_0 \quad (\text{B1})$$

where the tensor operators are defined by the tensor product of the orbital and spin operators (see the previous Appendix)

$$T_{L\gamma=1,\lambda\mu} = i^L f_L(r) (Y_L \times \sigma)_{\lambda\mu} \quad (\text{B2})$$

with $\lambda = 0, 1, 2, \dots, |\lambda - 1| \leq L \leq \lambda + 1$ and parity $\pi = (-1)^L$ and

$$T_{L\gamma=0,\lambda=L\mu} = i^L f_L(r) Y_{\lambda\mu} \quad (\text{B3})$$

for $\lambda = L = 0, 1, 2, \dots$, and $g_{L\gamma\lambda}$ is the strength of the interaction in the channel $(L\gamma)\lambda$. The actual values of $g_{L\gamma\lambda}$ are adjusted to reproduce the experimental data, either the energy of the low-lying states or the giant resonances, for each set of excitations.

The matrix element of a two-body interaction (B1), between particle-hole states may be written in terms of the matrix elements between two-particle configurations:

$$\langle pn^{-1} : J|V|p'n'^{-1} : J \rangle = - \sum_{J'} (2J' + 1) \begin{Bmatrix} p & n & J \\ p' & n' & J' \end{Bmatrix} \langle pn' : J'|V|p'n : J' \rangle \quad (\text{B4})$$

Therefore, the matrix element of the interaction in the particle representation is of the form

$$\begin{aligned} \langle pn' : J'|V|p'n : J' \rangle &= \sum_{L\gamma\lambda} g_{L\gamma\lambda} \begin{Bmatrix} p' & n & J' \\ n' & p & \lambda \end{Bmatrix} (2\lambda + 1)^{-1/2} (-1)^{\lambda+p'+n'+J'} \\ &\langle p||T_{L\gamma\lambda}||p' \rangle \langle n' ||T_{L\gamma\lambda}||n \rangle \end{aligned} \quad (\text{B5})$$

and, by writing the spin scalar ($\gamma = 0$) and spin vector ($\gamma = 1$) tensor components explicitly one has:

$$\begin{aligned} \langle pn' : J'|V|p'n : J' \rangle &= \sum_{L\gamma\lambda} g_{L\gamma\lambda} \begin{Bmatrix} p' & n & J' \\ n' & p & \lambda \end{Bmatrix} (2\lambda + 1)^{-1/2} (-1)^{\lambda+p'+n'+J'} \\ &(\delta_{\gamma,0}\delta_{L,\lambda} \langle p||i^L f_L(r)Y_L||p' \rangle \langle n' ||i^L f_L(r)Y_L||n \rangle \\ &+ \delta_{\gamma,1}\delta_{L,\lambda\pm 1} \langle p||i^L f_L(r)(Y_L \times \sigma)_\lambda||p' \rangle \langle n' ||i^L f_L(r)(Y_L \times \sigma)_\lambda||n \rangle) \end{aligned} \quad (\text{B6})$$

The determination of the amplitudes $C^{(k)}(pn, J^\pi)$ leads to the calculation of the transition amplitudes

$$\rho(pn; 0 \rightarrow J_f^\pi, k) = \delta_{\lambda J_f} C^{(k)}(pn, J^\pi) \quad (\text{B7})$$

Then, with these transition amplitudes, the matrix elements needed to calculate the neutrino-nucleus cross section are written

$$M_{(L\gamma)\lambda}(q) = \sum_{pn} \frac{1}{\sqrt{2\lambda + 1}} F(pn, qL) G(pn, L\gamma, \lambda) \rho(pn; 0 \rightarrow J_f^\pi, k) \quad (\text{B8})$$

and they are functions of the lepton momentum transfer q .

APPENDIX C: FORM FACTORS

To obtain the factors λ_τ and $\lambda_{\sigma\tau}$ of Eq.(7) we expand the leptonic and hadronic currents of the effective weak Hamiltonian, in terms of the momentum transfer q . By keeping contributions up to the order $\frac{1}{M_N}$, where M_N is the nucleon mass, the effective, minimal, weak Hamiltonian is written

$$H_{\text{weak}} = -\frac{G_F}{\sqrt{2}} \cos \theta_C [J^\mu j_\mu] \quad (\text{C1})$$

where j_μ is the lepton current

$$j_\mu = \bar{\psi}_e \gamma_\mu (1 + \gamma_5) \psi_\nu \quad (\text{C2})$$

and J^μ is the nucleon current in the limit of low momentum, with components

$$\begin{aligned} J^0 &= f_V(q) - \frac{1}{2M} f_A(q) (\sigma \cdot \mathbf{q}) \\ \mathbf{J} &= -i f_A(q) \sigma + \frac{1}{2M_N} (f_V(q) - 2M_N f_W(q)) (\sigma \times \mathbf{q}) + i f_V(q) \frac{\mathbf{q}}{2M_N} \end{aligned} \quad (\text{C3})$$

After some straightforward algebra, the calculation of the matrix elements of Eq.(2) yields

$$\begin{aligned}\lambda_\tau &= f_V^2(q)(1 + \cos\theta) \left[1 + 2 \left(\frac{E_e - E_\nu}{2M_N} \right) \right] \\ \lambda_{\sigma\tau} &= f_A^2(q) \left[\left(1 - \frac{1}{3} \cos\theta \right) + \frac{2}{3} \left(\frac{E_e - E_\nu}{2M_N} \right) (1 + \cos\theta) - \frac{4}{3} \left(\frac{E_e + E_\nu}{2M_N} \right) \left(\frac{f_V(q) - 2M_N f_W(q)}{f_A(q)} \right) (1 - \cos\theta) \right], \\ \lambda_\Lambda &= 4f_A^2(q) \left[\cos\theta + \left(\frac{E_l - E_\nu}{2M_N} \right) (1 + \cos\theta) + \left(\frac{E_l + E_\nu}{2M_N} \right) \left(\frac{f_V(q) - 2M_N f_W(q)}{f_A(q)} \right) (1 - \cos\theta) \right].\end{aligned}\quad (C4)$$

which agrees with the results of [14, 15]. The nucleon form-factors, for the axial(A), vector(V), and weak-magnetic(W) terms, $f_{V,A,W}$, have the following momentum dependence [15]

$$\begin{aligned}f_A(q) &= -\frac{1.262}{\left(1 + \frac{q^2}{(1.032\text{GeV})^2} \right)^2} \\ f_V(q) &= \frac{1}{\left(1 + \frac{q^2}{(0.84\text{GeV})^2} \right)^2} \\ f_W(q) &= -\frac{3.706}{2M_N} f_V(q)\end{aligned}\quad (C5)$$

In the above equations we have neglected pseudo-scalar terms, because they are smaller than the included terms by factors of the order $\frac{1}{M_N}$.

-
- [1] A. B. Balantekin and G. M. Fuller, *J. Phys. G* **29**, 2513 (2003)
 - [2] A. B. Balantekin and H. Yuksel, *New J.Phys.* **7**, 51 (2005)
 - [3] Y. Z. Qian et al, *Phys. Rev. Lett.* **71**, 1965 (1993)
 - [4] Q. R. Ahmad et al., *Phys. Rev. Lett.* **89**, 011301 (2002)
 - [5] Y. Fukuda et al., *Phys. Rev. Lett.* **81**, 1562 (1998)
 - [6] J. Bahcall, M. H. Pinsonneault and S. Basu, *Astrophys. J.* **555**, 990 (2001)
 - [7] J. Bahcall and C. Peña-Garay, *New J. Phys.* **6**, 63 (2004)
 - [8] H. Ejiri, *Phys. Rep.* **338**, 265 (2000).
 - [9] J. D. Vergados, *Phys. Rep.* **361**, 1 (2002).
 - [10] G. M. Fuller, W. C. Haxton and G. C. McLaughlin, *Phys. Rev. D* **59**, 085005 (1999)
 - [11] S. R. Elliot, *Phys. Rev. C* **62**, 065802 (2000)
 - [12] A. J. Noble; Proceedings of the Symposium *Physics in Collision*, Annecy, France, June 26-29, 2007.
 - [13] J. Engel, G. C. McLaughlin and C. Volpe, *Phys. Rev. D* **67**, 013005 (2003)
 - [14] M. Fukugita, Y. Kohyama, K. Kubodera and T. Kuramoto, *Astrophys. J.* **337**, 59 (1989)
 - [15] T. Kuramoto, M. Fukugita, Y. Kohyama and K. Kubodera, *Nucl. Phys. A* **512**, 711 (1990)
 - [16] C. Volpe, *J. Phys. G* **30**, L1-L6 (2004); *ibid* hep-ph/0303222.
 - [17] A. Bohr and B. Mottelson, *Nuclear Structure vol. 2*, Benjamin Readings, M. A, (1975).
 - [18] A. C. Hayes. APS Meeting Abstracts, 202 (1997).
 - [19] A. C. Hayes and I. S. Towner, *Phys. Rev. C* **61**, 044603 (2000).
 - [20] E. Kolbe and K. Langanke, *Phys. Rev. C* **63**, 025802 (2001).
 - [21] E. Kolbe, K. Langanke and P. Vogel, *Phys. Rev. D* **66**, 013007 (2002).
 - [22] J. Blomqvist, O. Civitarese, E. Kirchuk, R. J. Liotta, T. Vertse, *Phys. Rev. C* **53** (1996) 2001.
 - [23] O. Civitarese and M. Gadella, *Phys. Rep.* **396**, 41 (2004).
 - [24] A. Volya and V. Zelevinsky, *Phys. Rev. C* **67**, 054322 (2003) and references therein.
 - [25] R. Id Betan, R. J. Liotta, N. Sandulescu and T. Vertse, *Phys. Rev. Lett.* **89**, 042501 (2002).
 - [26] T. Vertse, P. Curutchet, O. Civitarese, L. S. Ferreira and R. J. Liotta, *Phys. Rev. C* **37**, 876 (1988).
 - [27] J. Suhonen and O. Civitarese, *Phys. Rep.* **300**, 123 (1998)
 - [28] T. Berggren, *Nucl. Phys. A* **109**, 265 (1968).
 - [29] R. J. Liotta, E. Maglione, N. Sandulescu and T. Vertse, *Phys. Lett. B* **367**, 1 (1996).
 - [30] R. Id Betan, R. J. Liotta, N. Sandulescu, T. Vertse and R. Wyss, *Phys. Rev. C* **72**, 054322 (2005).
 - [31] T. Berggren and P. Lind, *Phys. Rev. C* **47**, 768 (1993).
 - [32] T. Vertse, R. J. Liotta and E. Maglione, *Nucl. Phys. A* **584**, 13 (1995).
 - [33] P. Curutchet, T. Vertse and R. J. Liotta, *Phys. Rev. C* **39**, 1020 (1989).
 - [34] L. Gr. Ixaru, M. Rizea and T. Vertse, *Comput. Phys. Commun.* **85**, 217 (1995).

- [35] P. Alexa, J. Kvasil and R. Sheline, Phys. Rev. C **55**, 3170 (1997).
- [36] T. Berggren, Phys. Lett. **B 73**, 389 (1978).
- [37] K.Langanke et al., Phys. Rev. Lett. **100**, 011101 (2008).
- [38] R. Lazauskas and C. Volpe, Nucl. Phys. **A 792**, 219 (2007).
- [39] A. Bohr and B. Mottelson, Nuclear Structure vol. I, W. A. Benjamin Inc., M. A, (1975).